The Effect of Near-Surface Winds on Surface Temperature and Dust Transport on Venus

Maxence Lefèvre, Sébastien Lebonnois, Aymeric Spiga, François Forget

JGR Planets

RESEARCH ARTICLE
10.1029/2025JE009133

The Effect of Near-Surface Winds on Surface Temperature and Dust Transport on Venus

Maxence Lefèvre[1], **Sébastien Lebonnois**[2], **Aymeric Spiga**[2], **and François Forget**[2]

[1]Centre National de la Recherche Scientifique, LATMOS/IPSL, Sorbonne Université, UVSQ, Université Paris-Saclay, Paris, France, [2]LMD/IPSL, CNRS, Sorbonne Université, École Normale Supérieure, Université PSL, École Polytechnique, Institut Polytechnique de Paris, Paris, France

Abstract The knowledge of the Venus near-surface atmosphere is sparse. Few spacecrafts landed on the surface and measured winds with amplitudes below 1 m/s. The diurnal cycle of the wind amplitude and orientation is not known. Recent numerical simulations showed that slope winds along topographic structures could strongly impact the direction of winds. This study presents the first mesoscale modeling of such winds on Venus. A change of direction is occurring during the day in the main slopes, with upslope winds at noon due to solar heating and downslope winds at night. This is due to efficient IR cooling of the surface during the night, being colder than its surroundings slope atmospheric environment and leading to displacement of air. The temperature is impacted by the adiabatic cooling/warming induced by those winds. A strong heating effect is occurring for the downslope winds, leading to an anti-correlation between the surface temperature diurnal amplitude and the topography. This diurnal amplitude reaches 4 K in the plains and below 1 K in the mountains. The saltation of sediment by those winds was also quantified, with a higher probability at night along the slopes on the western flanks.

Plain Language Summary Nighttime downslope winds are important meteorological features. It is the strongest land wind measured on Earth, whereas on Mars it is a key phenomenon of the dynamics of the near-surface region. On Venus, the importance of such is not known due to the lack of measurements at the surface. To investigate this topic, we use a regional model for the first time on Venus. During the day, there is a strong change of direction of these winds, going upslope at noon due to solar heating and downslope at night due to IR cooling. This change of direction particularly occurs near the Equator, where the solar flux is stronger. The temperature will also be impacted by adiabatic cooling/warming by those winds. A strong heating effect is associated with the downslope winds. The surface temperature diurnal amplitude is stronger in the plain than in the mountains, reaching respectively 4 K versus below 1 K. The surface temperature is therefore not only controlled by elevation but also by the slope. The lifting of sediment was also quantified with our model. A higher probability was estimated at night along the slopes. The western flank of the mountains would be preferable locations for sediment transport.

Key Points:

- For the first time, a Venus mesoscale climate model is used to simulate the local near-surface winds dynamics
- Modeled slope winds are changing direction during the day due to IR cooling, and are mitigating the surface temperature diurnal amplitude
- Regional wind is strong enough to lift dust, with a third of the domain above the lowest particle saltation threshold

Supporting Information:

Supporting Information may be found in the online version of this article.

Correspondence to:

M. Lefèvre,
maxence.lefevre@latmos.ipsl.fr

Citation:

Lefèvre, M., Lebonnois, S., Spiga, A., & Forget, F. (2025). The effect of near-surface winds on surface temperature and dust transport on Venus. *Journal of Geophysical Research: Planets*, *130*, e2025JE009133. https://doi.org/10.1029/2025JE009133

Received 4 APR 2025
Accepted 26 AUG 2025

Author Contributions:

Conceptualization: Maxence Lefèvre
Investigation: Maxence Lefèvre
Methodology: Maxence Lefèvre
Validation: François Forget
Visualization: Maxence Lefèvre
Writing – original draft: Maxence Lefèvre, Sébastien Lebonnois, Aymeric Spiga
Writing – review & editing: Maxence Lefèvre, Sébastien Lebonnois, Aymeric Spiga, François Forget

1. Introduction

The knowledge of the near-surface winds and temperature on Venus is essential, as the interaction between the surface and atmosphere is one of the objectives of future missions, with DAVINCI planning to measure temperature and winds near the surface (Garvin et al., 2022), and VERITAS and EnVision observing aeolian features (Ghail et al., 2018). In addition, several projects of long-duration landers at the surface of Venus are in development, like the Seismic and Atmospheric Exploration of Venus (SAEVe) concept (Kremic et al., 2020). Characterization of the near-surface winds is also crucial to better understand the deep atmosphere dynamics and to constrain lander trajectories/landing (Knicely et al., 2023).

Only a limited number of probes have been able to collect data on the near-surface of Venus. At the surface, only VENERA-9 and 10 directly measured the wind for respectively 49 min and 90 s (Avduevskii et al., 1977), and several other probes like VENERA-13 and 14 indirectly measured the wind speed (Ksanfomaliti et al., 1983). The amplitudes of the measured wind speeds are less than 2 m s^{-1} below 100 m (Lorenz, 2016), and typical values are below 0.5 m s^{-1} below 1 m. The diurnal cycle of the amplitude and orientation of the wind near the surface of Venus is not known, nor are the effects of the topography. The diurnal amplitude of the surface temperature can potentially impact the gas buffering at the surface and have implications on the surface evolution (Jakosky, 1984).

Due to the thick clouds and hot temperatures, remote surface temperature measurements are scarce. The surface temperature diurnal variation has been calculated using a variety of methods. It was estimated to be below 1 K based on radiative transfer modeling (Lewis, 1971; Stone, 1975), around 15 K (Bohachevsky, 1973) and below 3 K (Lebonnois et al., 2018) with Global Circulation Models (GCM) simulations, and about 6 K due to Planetary Boundary Layer dynamics (Gierasch et al., 1997). Two dune fields have been observed with Magellan radar measurements (Greeley et al., 1992), although the lack of knowledge about the spatial and temporal distribution of winds complicates the interpretation of sediment transport.

The Venus Planetary Climate Model (Venus PCM, formerly called the IPSL Venus GCM) simulations showed that the diurnal cycle of the planetary boundary layer (PBL) activity is correlated with the diurnal cycle of surface winds (Lebonnois et al., 2018). The global model predicted observed katabatic winds at night and anabatic winds during the day along the slopes of high-elevation terrains, resulting in a deeper PBL depth at midday.

Katabatic winds are an atmospheric flow formed when cooled dense air is accelerated downhill by gravity, overcoming the opposing along-slope pressure gradient (Mahrt & Larsen, 1990). These winds are particularly strong over ice-covered Greenland and the Antarctic, where the near-surface temperature inversions in winter reach 25 K, reaching typically 20 m s^{-1} with gusts exceeding 35 m s^{-1} (Nylen et al., 2004), around four times the equivalent outside polar regions. On Mars, the diurnal cycle of the surface temperature is three times larger than on Earth due to low thermal inertia and short radiative timescales of the thin CO_2 atmosphere, causing rapid transition from afternoon superadiabatic gradients to nighttime super-stable inversion and leading to winds up to 40 m s^{-1} (Richardson et al., 2007; Richardson & Newman, 2018; Spiga & Forget, 2009) with typical temperature inversion between 20 and 30 K (Spiga, 2011).

In this study, for the first time, we use mesoscale modeling to simulate the diurnal cycle of Venus' near-surface dynamics and especially estimate the influence of the topography on the surface temperature and saltation. Regional modeling has been extensively used to study these topics for the Earth (Mikkola et al., 2023; Schmidli et al., 2018) and Mars (Hernández-Bernal et al., 2022; Lange et al., 2023; Montlaur et al., 2024; Rafkin et al., 2016; Spiga & Smith, 2018).

In Section 2, the model is described. In Section 3, the impact of topography on the near-surface wind amplitude and direction is discussed. In Section 4, the effect of the slope winds on the surface temperature is assessed. The contribution of these winds to the transport of sediment is estimated in Section 5. Our conclusions are summarized in Section 6.

2. Modeling

The LMD Venus mesoscale model (Lefèvre et al., 2020) is based on the dynamical core of the Advanced Research Weather-Weather Research and Forecast (hereinafter referred to as WRF) terrestrial model (Skamarock & Klemp, 2008). The WRF dynamical core integrates the fully compressible non-hydrostatic Navier-Stokes equations over a specified area of the planet and uses mass-coupled atmospheric variables (winds and potential temperature) with an explicitly conservative flux-form formulation of the fundamental equations to ensure the conservation of mass, momentum, and entropy (Skamarock & Klemp, 2008).

The solar and IR heating rates are calculated using the Venus PCM radiative transfer scheme (Haus et al., 2015; Lebonnois et al., 2015) solar rates look-up tables. The horizontal grid spacing for a mesoscale simulation is generally set to several tens of kilometers, and the convective turbulence in the planetary boundary layer and the cloud layer is not resolved. Therefore, similarly to what is done in global modeling, the LMD Venus mesoscale model uses a subgrid-scale parameterization for turbulent mixing. As in the Venus PCM, for mixing by smaller-scale turbulent eddies, the formalism of level 2.5 of Mellor and Yamada (1982) is adopted, which calculates with a prognostic equation the turbulent kinetic energy and mixing length. This scheme is taken from the LMDz model and is fully described in Appendix B of Hourdin et al. (2002). It has been used extensively in Martian conditions (Forget et al., 1999), computing temperature and wind with consistent in situ measurements. For Venus, no measurements exist to tune this scheme, but the temperature and winds close to the surface are qualitatively consistent with calculations in the PCM (Lebonnois et al., 2018). A simple dry convective adjustment is used to compute mixed layers in convectively unstable temperature profiles.

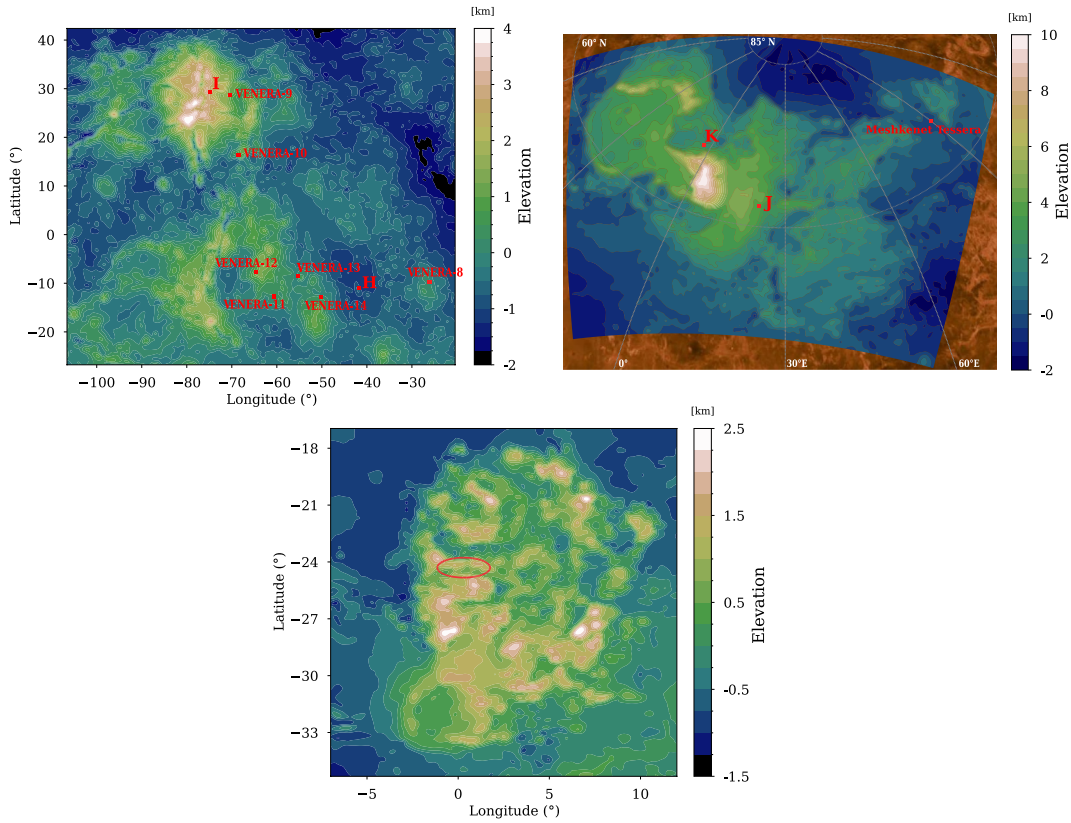

Figure 1. Elevation map of the Equatorial (top-left) and Polar (top-right) and Alpha Regio (bottom) domains with the location of the seven VENERA spacecrafts landing sites and five other points of interest represented by red squares. The red ellipse represents the landing area of DAVINCI (Garvin et al., 2022).

2.1. Simulation Settings

The three selected spatial domains shown in Figure 1 were built using Magellan topography data (Ford & Pettengill, 1992) and Pioneer Venus data (Pettengill et al., 1980). The Equatorial domain (top-left) was chosen to incorporate the seven VENERA landing sites considered in this study, all located in a rather confined location, within 80,000 km^2. The characteristics of these landing sites are summarized in Table 1. The Polar domain (top-right) was chosen to incorporate Ishtar Terra, where Maxwell Montes, the highest mountain of Venus, is present with 10 km of altitude and slopes reaching 45°. This domain was calculated using polar projection. The third domain (bottom) is centered over Alpha Regio, where DAVINCI will land (Garvin et al., 2022). To have an accurate resolution of the slopes with a reasonable computational time, the horizontal resolution of the Equatorial domain is set to 20 km, 15 km for the Polar domain and 5 km for Alpha Regio. Given the horizontal resolutions involved, the dynamical timestep for mesoscale integrations is set to 8 s to ensure numerical stability. The vertical grid is the same as in Lefèvre et al. (2020), with 150 levels from the surface to 90 km.

The settings of the simulations shown in this study are similar to the ones in Lefèvre et al. (2020). The albedo, thermal inertia, and aerodynamic roughness height are set constant over the whole domain at respectively 0.5, 2000 J m^{-2} s$^{-1/2}$ K^{-1} and 0.01 m. An 11-layer soil model is for the thermal conduction in the soil (Hourdin et al., 1993). The horizontal boundary conditions have been chosen as 'specified', that is meteorological fields are extracted from the Venus PCM simulations (Garate-Lopez & Lebonnois, 2018) and interpolated both on the vertical grid, accounting for the refined topography of the mesoscale domain, and on the temporal dimension, accounting for the evolution of those fields over the low dynamical timestep in mesoscale integrations, ensuring the planetary-scale super-rotation of the Venusian atmosphere is well represented. The boundary fields are updated at a frequency of a 1/100 Venus day, enabling a correct representation of the large-scale variability simulated by GCM at the boundaries of the mesoscale domain. Between the mesoscale domain and the specified boundary fields, a relaxation zone set to 5 grid points is implemented to allow for the development of the

Table 1
Summary of the VENERA 8 to 14 Landing Site Informations and Wind Amplitude Measurements

Mission	Location	Measurements (m s^{-1})
VENERA-8	10.70°S, 335.25°E	0.25 ± 0.5[a]
	altitude: 193.8 m; LT: early morning[a]	
VENERA-9	31.01°N, 291.64°E	1.2 ± 1.0[a]
	altitude: 1110 m; LT: early afternoon[a]	0.4–0.7[b]
VENERA-10	15.42°N, 291.51°E;	0.6 ± 1.0[a]
	altitude: −87.1 m; LT: early afternoon[a]	0.8–1.3[b]
VENERA-11	14°S, 299°E	<1.2[c]
	altitude: 234.1 m; LT: mid-morning[a]	
VENERA-12	07°S 294°E;	<1.2[c]
	altitude: 594.5 m; LT: mid-morning[a]	
VENERA-13	07.05°S 303°E;	0.51(+0.19/−0.26) to 0.57(+0.43/−0.29)[d]
	altitude: 429.6 m; LT: mid-morning[e]	
VENERA-14	13.25°S 310°E;	0.35(+0.65/−0.18) to 0.39(+0.61/−0.200)[d]
	altitude: 485.4; LT: mid-morning[e]	

[a]Kerzhanovich & Marov, 1983. [b]Avduevskii et al., 1977. [c]Kerzhanovich et al., 1980. [d]Ksanfomaliti et al., 1983. [e]Moroz, 1983.

mesoscale circulations inside the domain while keeping prescribed PCM fields at the boundaries (Skamarock & Klemp, 2008). Simulations were performed for a whole Venus day, that is, 117 Earth days.

3. Diurnal Variability of Wind Amplitude and Direction

Figure 2 shows the sunflower wind chart of the 10 m horizontal wind (m s^{-1}) for different locations pointed on Figure 1. For the 7 VENERA landing sites, the horizontal wind amplitude resolved from the mesoscale model is below 1.6 m s^{-1} and around 0.5 m s^{-1} in the late morning/early afternoon window, consistent with the in situ measurements all in this local time window (Table 1). The amplitude of the wind varies during the day, except for the VENERA-10 location (C) and the Equatorial plain point (H). The landing site of VENERA-10 is between Phoebe and Beta Regio, a region where there is a strong convergence of winds. The wind is stronger at night and weaker around midday. For most of the points of interest, there is also a change in the wind direction, with a 180° shift between midnight and midday. The 7 VENERA landing points are located near mountains, where slope winds may impact the direction of winds. The VENERA-10, H and K locations have a more scattered change of direction during the day. Points I, J, and K are at higher altitudes than the other locations, resulting in stronger amplitudes.

The amplitude distribution of the horizontal wind at 2, 10 and 100 m for the two domains at midday and midnight are shown in Figures S1 and S2 in Supporting Information S1. The horizontal wind at 2 m (left) displays an amplitude between 0 and 1.5 m s^{-1}, with 80% for both midday and midnight of its amplitude below 0.5 m s^{-1}. At 10 m, winds can reach 1.75 m s^{-1}, but with still 95% below 1 m s^{-1} at midday, against 90% at midnight. At 100 m, the wind's amplitude is increasing, reaching values as high as 3.0 m s^{-1}. However, around 75% is below 1 m s^{-1} at midday and 60% at midnight. At midday, 95% of the horizontal wind is below 1.5 m s^{-1}. These distributions at midday are consistent with the probability distribution estimated from the in situ measurements at similar local time and latitude range (Lorenz, 2016). The difference between the two local times in the Equatorial region is representative of the diurnal cycle of the surface wind discussed in this study, with stronger wind at night. At 150 m of altitude, the large-scale winds reached 2 m s^{-1} in the Equatorial domain and 3 m s^{-1} in the North Pole, inferior by 25% to the mesoscale winds. In Alpha Regio (Figure S3 in Supporting Information S1), the distribution is similar to the Equatorial domain, with around 80% for both midday and midnight of its amplitude below 0.5 m s^{-1}. However, the wind amplitude is slightly stronger by day due to the presence of Lavinia Planitia in the vicinity of Alpha Regio, a 2,000 km wide depression two km below, where anabatic winds are heading toward the mountain.

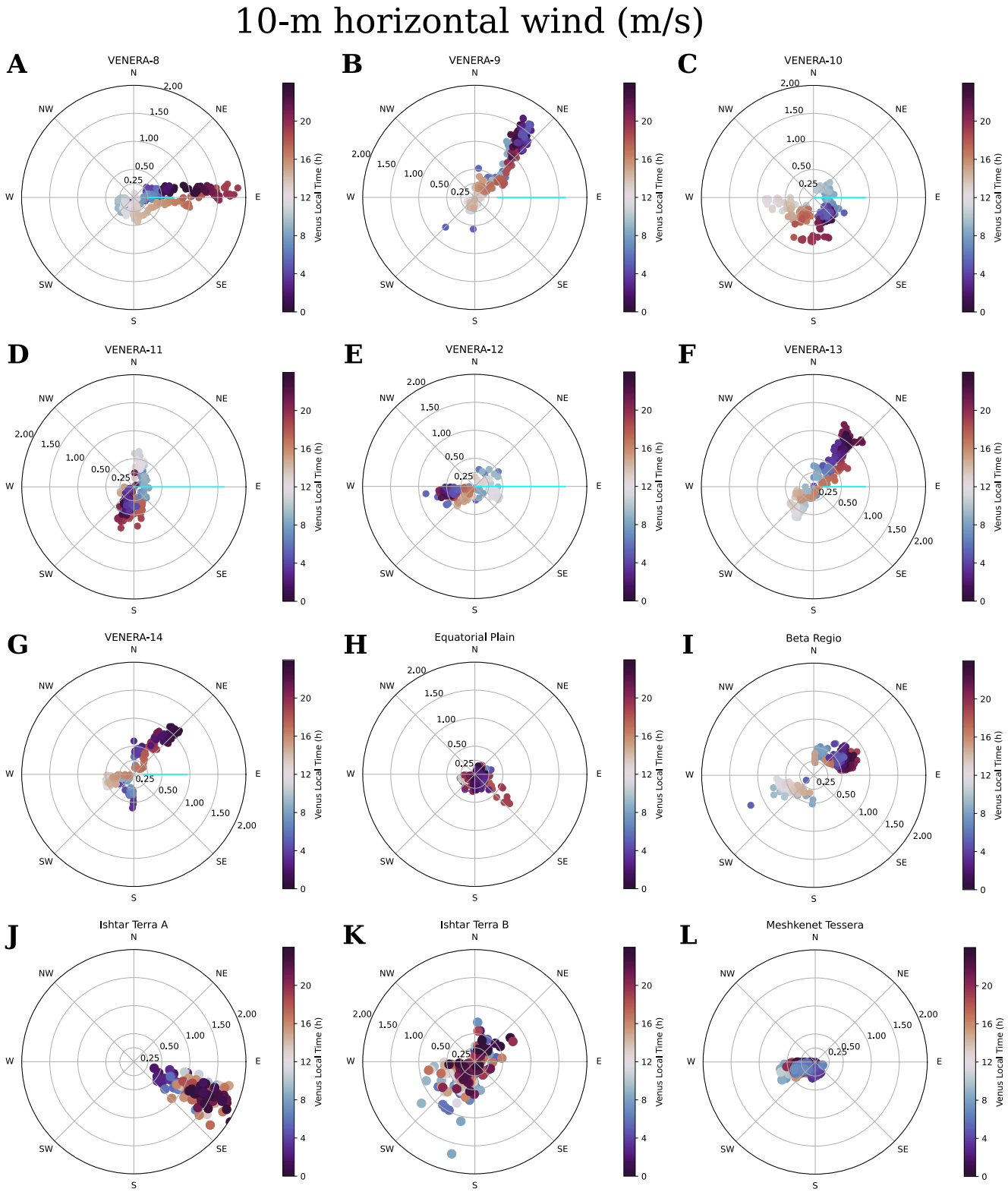

Figure 2.

Figure 3 shows snapshots of the 10 m wind directions at midnight (left column) and midday (right column), focused on Phoebe Regio, Beta Regio, Ishtar Terra and the whole Alpha Regio domain. Maps of the entire Equatorial and Polar domain are shown in Figure S4 in Supporting Information S1. In the first two lines in the Equator domain, the change of direction along a Venus day is visible with anabatic (upslope) winds at midday and katabatic (downslope) winds at midnight, especially on the eastern flanks of Beta Regio and Poebe Regio. This change of direction in the slope is due to a temperature inversion, specific to the environment. During the day, the solar flux is heating the flanks of a mountain, reaching a typical value at the Equator around 90 W m^{-2} at noon, consistent with in situ measurements (Moroz, 1983). In this environment, this will lead to the surface of the mountain being hotter than its immediate atmospheric surroundings in the same isobar, and therefore less dense, leading to anabatic winds. At night, the surface is cooling more efficiently by the IR cooling than the atmosphere at the same isobar, typically $-1{\cdot}10^{-6}$ K s^{-1} on the slope against $-1{\cdot}10^{-7}$ K s^{-1} in the close atmosphere, leading to an immediate atmospheric environment colder and denser than its surroundings, engendering katabatic winds. This change of direction is consistent with the output of the Venus PCM (Lebonnois et al., 2018). Over Ishtar Terra, however, there are no changes of direction. The wind is constantly going downslope due to IR radiation cooling constantly during the day. The solar flux below 30 W m^{-2} on Ishtar Terra southern flank is too weak to engender anabatic winds. On Maxwell Montes, the highest mountain, the wind goes over the mountain throughout the day, reaching 3.0 m s^{-1}.

Several layers with significant decreases in surface emissivity and high radar reflectivities were observed at several altitudes on high-relief (Brossier et al., 2020). The main hypothesis is the presence of strongly dielectric compounds, as ferroelectric materials (Treiman et al., 2016) from atmosphere-surface interaction and/or precipitating minerals. Strezoski and Treiman (2022) reanalyzed Magellan data and showed that the emissivity drop altitudes vary over Maxwell Montes, suggesting that the atmosphere is progressively depleting in precipitable material as it crosses the mountain from south-east. The wind direction over Maxwell Montes is consistent with the atmospheric precipitate hypothesis, in addition to atmosphere–rock chemical reactions, to interpret Magellan radar features.

In Alpha Regio, there is also the presence of slope winds, katabatic by night and anabatic by day, especially on the boundary of the mountains. Due to the complex terrain, several points of wind convergence are present. The large-scale wind on the western side of the mountain is going east, contrary to the equatorial region, where the wind is globally western. This difference is due to Lavinia Planitia in the vicinity of Alpha Regio is driving the direction of the large-scale wind in this region.

The amplitude of slope winds is typically around 1 m s^{-1} in the Equatorial region, one order of magnitude below its Earth and Martian equivalent, which reaches several tens of m s^{-1}. From McNider (1982), a frictionless upper limit value for the acceleration of the wind Γ along a slope of inclination α is

$$\Gamma = \frac{g \sin(\alpha)\Delta T}{\langle T \rangle} \tag{1}$$

where ΔT is the near-surface temperature inversion, $\langle T \rangle$ is the average near-surface temperature and g is the acceleration of gravity equal to 8.87 m s^{-2}. On Earth, typical radio-sounding profiles in the Sahara desert show at night a $\langle T \rangle$ equal to 285 K and a ΔT equal to 5 K between 0 and 250 m above the surface. For Mars at the same local time, $\langle T \rangle$ is equal to 175 K and ΔT 30 K between 0 and 250 m also at night (Spiga, 2011). On Venus, on Beta Regio the typical temperature value is 705 K with a ΔT around 0.6 K. For the same inclination, the acceleration of the wind on Earth will be half that on Mars, but 20 times larger than on Venus. Therefore, due to its larger temperature and more stable atmosphere, the amplitude of slope winds on Venus is smaller.

Figure 2. Sunflower wind chart of the 10 m horizontal wind for VENERA-8 (a), VENERA-9 (b), VENERA-10 (c), VENERA-11 (d), VENERA-12 (e), VENERA-13 (f) VENERA-14 (g) locations every 8 Venusian minutes (.i.e.). (h) is a point in the Equatorial plain near Phoebe Regio, and (i) is a point in the East flank of Beta Regio. (j) and (k) are two points on Ishtar Terra. (l) is located in Meskhenet Tessera where a dune field was observed (See Figure 1). The cyan lines represent the surface wind amplitude measured range for the VENERA landers in the late morning/early afternoon (Table 1). No directions were estimated for VENERA observations, the Eastern direction is for illustration only.

10.1029/2025JE009133

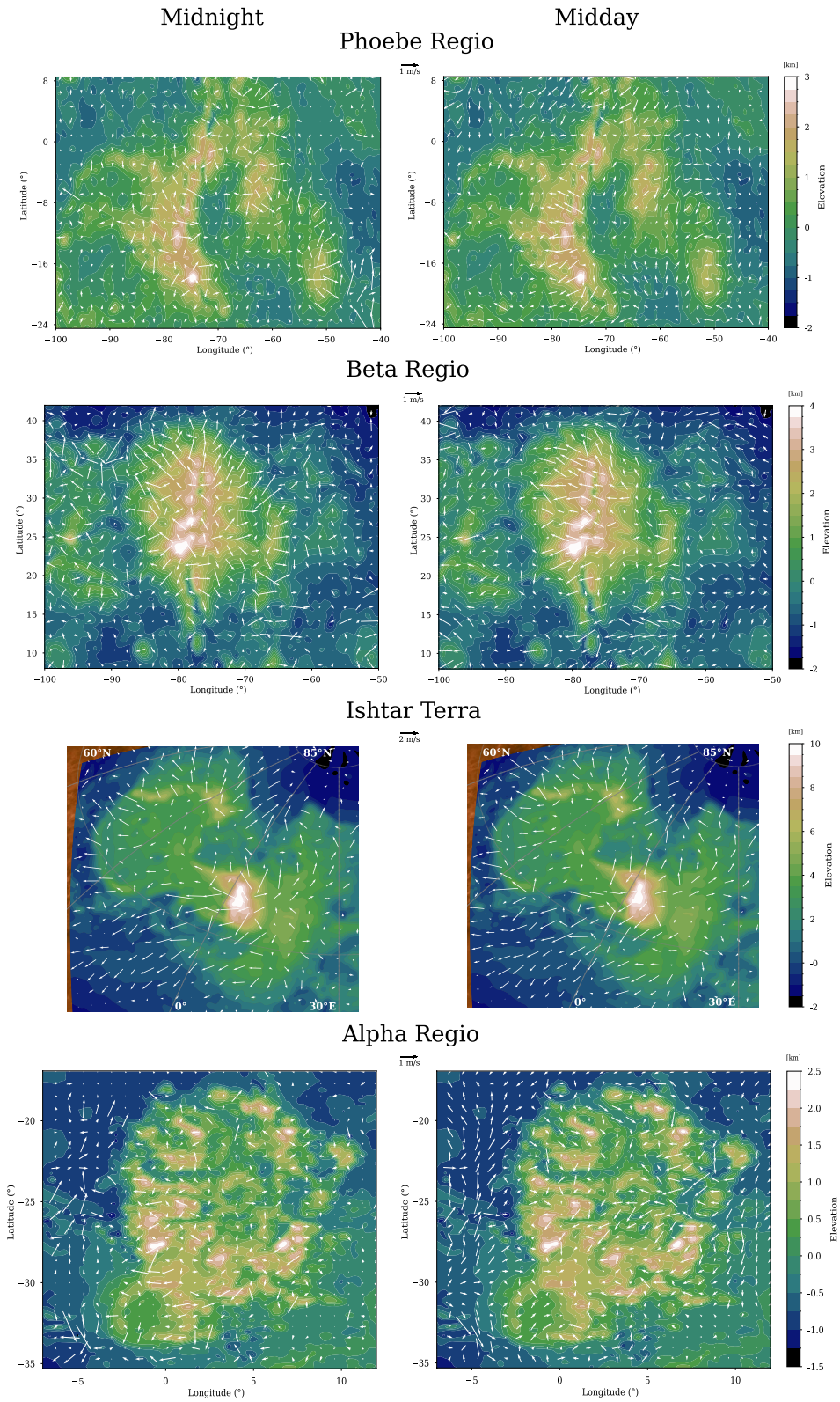

Figure 3. Snapshots maps of horizontal winds 10 m above the local surface (m s^{-1}) at midnight (left column) and midday (right column) in the center of the domain above Phoebe Regio, Beta Regio, Ishtar Terra and Alpha Regio.

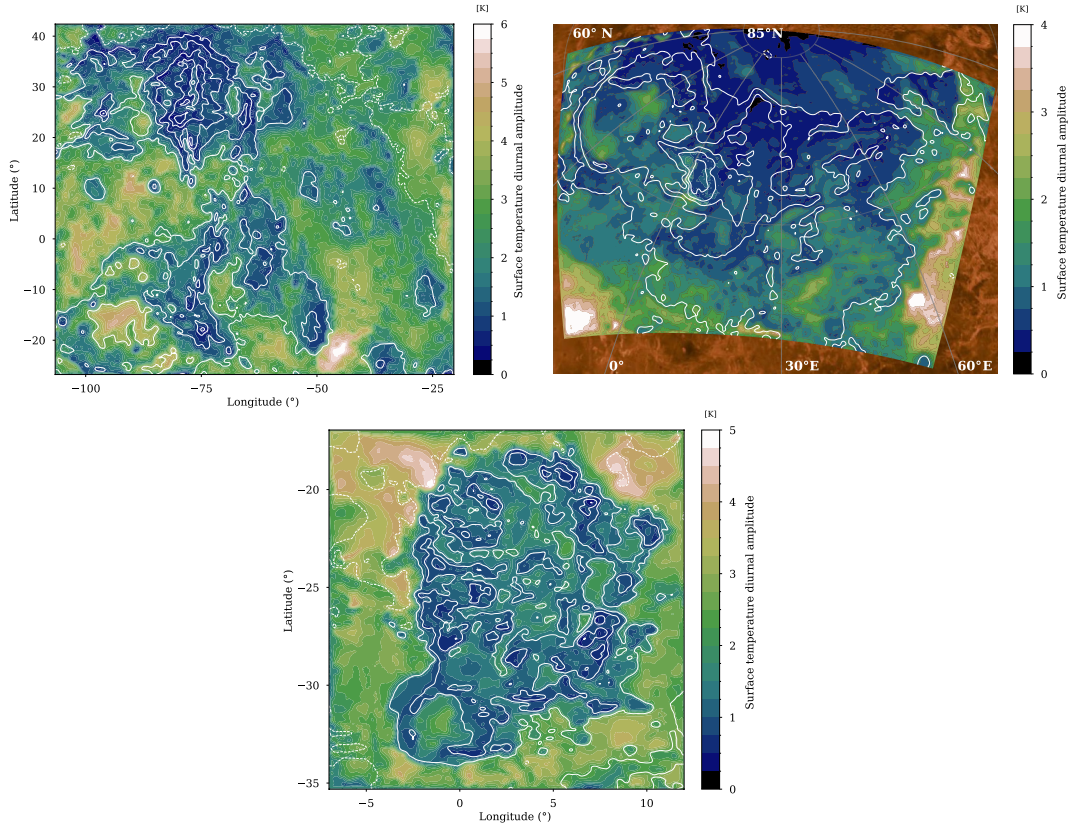

Figure 4. Map of the surface temperature diurnal amplitude (K) for Equatorial (top-left), Polar domain (top-right) and Alpha Regio (bottom). White contours represent the topography (Figure 1), every kilometer for the Equatorial domain, 2 km for the Polar domain and every 600 m for Alpha Regio.

4. Effect on Surface Temperature

On Venus, the surface temperature is mainly determined by the elevation and is in thermal equilibrium with the atmosphere (Lecacheux et al., 1993), both due to the high density of the latter, the low solar flux reaching the surface, and the absence of latent heat flux. On Mars, the surface is, within good approximation, in radiative equilibrium with solar illumination because the atmosphere is so thin. However, the environment of slope winds departs from this equilibrium due to adiabatic heating/cooling and affects the surface temperature (Spiga et al., 2011).

Figure 4 shows the surface temperature diurnal amplitude (K) for the three domains. The strong anti-correlation between surface temperature diurnal amplitude and topography is visible at the Equator and in Alpha Regio, where the low plains have a 4 K diurnal amplitude, whereas the high terrains have an amplitude below 1 K. In the Polar domain, there is no correlation between the topography and surface temperature diurnal amplitude. This amplitude is around 4 K in the low plains at 40° of latitude. At higher latitudes, the diurnal amplitude falls below 2 K due to the smaller solar heat flux.

On the equatorial plains and outside Alpha Regio, the 3–4 K surface diurnal amplitude is due to the solar heating during the day and the nighttime IR cooling. In the mountainous region, there is a third contribution. To understand the impact of slope wind on surface temperature, the induced adiabatic cooling/warming is calculated as follows (Spiga et al., 2011):

$$J_{adiab} = -\frac{g}{C_p} w \tag{2}$$

with g the acceleration of gravity, C_p the heat capacity set to typical Venus tropospheric value of 1000 J K^{-1}, and w the vertical wind component (m s^{-1}) resolved by the model. Katabatic winds will heat the parcel, and anabatic winds will cool the parcel. Figure 5 shows the maps of J_{adiab} at 2 m for the three domains at midnight and midday.

The vertical component of the wind at 2 m has an average value of −0.002 m s^{-1} with a standard deviation of 0.002 m s^{-1}, a maximum of 0.015 m s^{-1} and a minimum of −0.03 m s^{-1} for the Equatorial domain, averaged over the entire Venus day. For the Polar domain, the wind at 2 m has an average of −0.004 m s^{-1} with a standard deviation of 0.009 m s^{-1}, a maximum of 0.02 m s^{-1} and a minimum of −0.2 m s^{-1}. Diurnal variation of near-surface vertical wind for Beta Regio and the equatorial plain, point I and H in Figure 1, is shown in Figure S5 in Supporting Information S1. With these values of vertical wind, the slope wind adiabatic heating rates reach values of $-1{\cdot}10^{-7}$ and $1{\cdot}10^{-5}$ K s^{-1} in the Equatorial plain and Beta Regio respectively at night. Typical values of the nighttime longwave cooling rate on a slope are around $-1{\cdot}10^{-6}$ K s^{-1}, that is an order of magnitude lower than the slope wind rates. The timescale of radiative cooling is therefore longer and cannot balance the warming induced by katabatic adiabatic compression through vertical motion, leading to a decrease of the surface temperature diurnal amplitude in the slopes compared to plains.

This effect of slope on the temperature shows that near the Equator, the surface temperature is not only controlled by the elevation but also by the slope. This should be considered when measuring the surface properties like emissivity and thermal inertia. A Surface Brightness 4 K temperature anomaly was retrieved at the same latitude and altitude between a plain and a mountainous region (Mueller et al., 2020), possibly linked to a difference in surface temperature.

5. Eolian Transport

Only two prominent dune fields have been identified on Venus with the Magellan radar (Greeley et al., 1992), Algaonice at 25°S, 340°E covers some 1,300 km^2 with bright dunes of 0.5–5 km in length with a wavelength around 0.5 km, and Fortuna-Meskhenet at 67°N, 91°E with transverse dunes of 0.5–10 km long, 0.2–0.5 km wide and spaced by an average of 0.5 km. Several sites with micro-dunes or small-scale wind streaks have also been proposed (Bondarenko et al., 2006; Weitz et al., 1994), but the resolution of the Magellan radar was not high enough to confirm them.

Within the lowest portion of the planetary boundary layer, a semi-empirical logarithmic wind profile approximated by the Prandlt-von Kármán equation defining the friction velocity $u^\star$ is commonly used to describe the vertical distribution of horizontal mean wind speed:

$$u_\star = k\frac{u_z}{\ln(z/z_0)} \tag{3}$$

With the Von Kármán constant, k, equal to 0.4, the aerodynamic roughness height, z_0, is set to 1 cm, in the range of values estimated from Magellan radar measurements (Blumberg & Greeley, 1994). u_z is the horizontal wind at the altitude z.

Theoretical calculations and laboratory experiments estimated the threshold friction velocity $u_{\star t}$ for which the dust is to be lifted in Venus surface conditions to be minimum around 2.5 10^{-2} m s^{-1} (Gunn & Jerolmack, 2022; Iversen et al., 1976; Iversen & White, 1982). The stress associated $\tau = \rho \cdot u_{\star t}^2$, with ρ the density of the atmosphere, is about two times lower for Venus than for Earth, and three times lower than for Mars. Such a threshold value depends also on the density of the sediment, data that is not well-known yet. These thresholds are calculated for a 2.65 g cm^{-3} particle density, but no measurement exists for Venusian surface particles.

Figure 6 shows instantaneous maps of $u^\star$ from the 2-m wind for the three domains at midnight and midday. For the Equatorial domains, the median value of $u^\star$ is around 2 10^{-2} m s^{-1}, several orders of magnitude below Earth and Mars (Gunn & Jerolmack, 2022). The friction velocity is stronger at night due to higher horizontal wind amplitude. At midday, 33% of the domain have a $u^\star$ value above the 2.5 10^{-2} m s^{-1} $u_t^\star$ for particle of 75 μm, and 1% of the domain is above the 7 10^{-2} m s^{-1} $u_t^\star$ for particle of 10 μm or 1 mm. At night, it reaches 36% of the domain above the 75 μm $u_t^\star$ and 3% for 10 μm (or 1 mm) threshold. For the Polar domain, 43% at midday, and 46% at night of the domain above the 75 μm threshold, against 18% at midday and 19% at night above the 10 μm

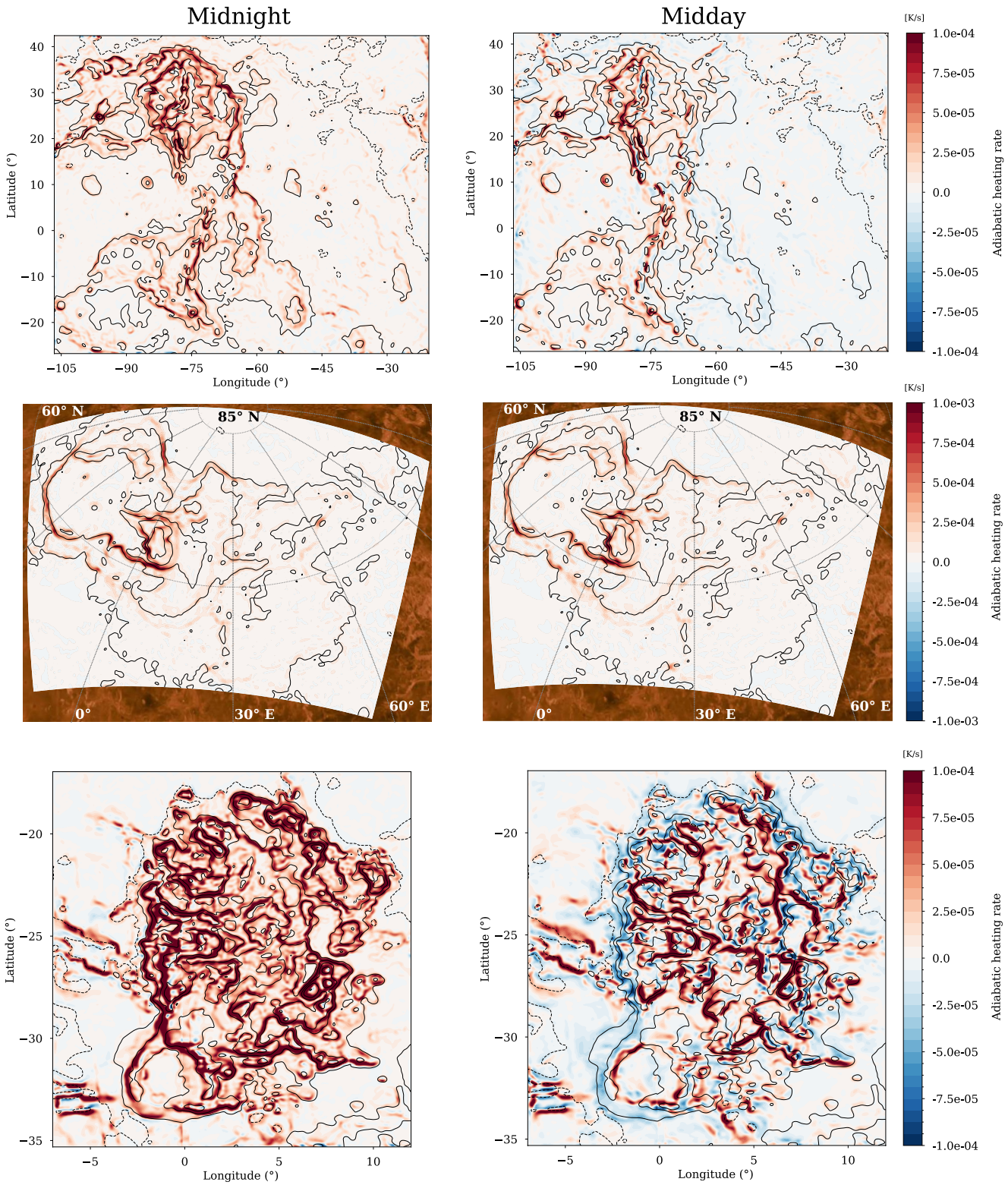

Figure 5. Top: Snapshots maps of the adiabatic heating rate of an atmospheric parcel with vertical wind velocity at 2 m above local surface J_{adiab} (K/s) at midnight (left) and midday (right) for the Equatorial (top) and Polar (center) domains and Alpha Regio (bottom). Black contours represent the topography (Figure 1), every kilometer for the Equatorial domain, 2 km for the Polar domain and every 600 m for Alpha Regio.

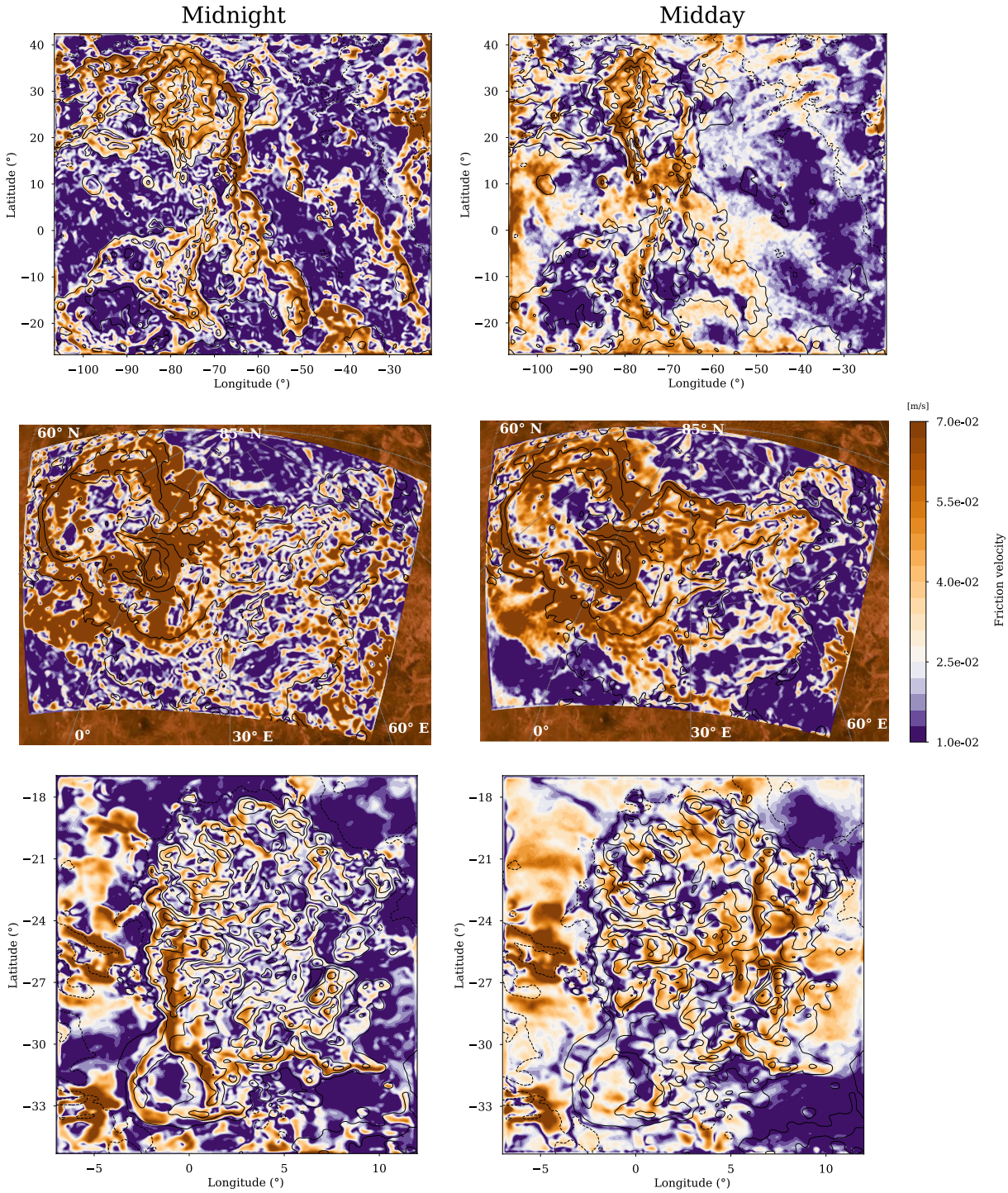

Figure 6. Map of the friction velocity u⋆ at midnight (left) and midday (right) for the Equatorial (top) and Polar (center) domains and Alpha Regio (bottom). Back contours represent the topography (Figure 1), every kilometer for the Equatorial domain, 2 km for the Polar domain and every 600 m for Alpha Regio.

threshold. In the Equator, some locations are above the saltation threshold both at midnight and midday. This is the case for the western flank of the mountains due to the western direction of the large-scale wind. The region at 12°N and −70° of longitude, between Phoebe Regio and Beta Regio, is also a region of interest for sedimentary transport, especially during the day, due to strong gap winds on the flat land between those two mountains (Figure 1). In Alpha Regio, at midnight 29% of the domain have a u⋆ value above the 2.5 10^{-2} m s^{-1} $u_t^\star$ for

particle of 75 μm, and 2% of the domain is above the 7 10^{-2} m s^{-1} $u_t^\star$ for particle of 10 μm or 1 mm, whereas at midday 45% and 2% are respectively above the 2.5 10^{-2} m s^{-1} and 7 10^{-2} m s^{-1} threshold.

In Fortuna-Meskhenet region, where dune fields were observed, the friction velocity is at the 0.025 m s^{-1} threshold, meaning that dust can be lifted in the area by regional slope winds. The dune field is composed of two main directions, with a southeast-to-northwest wind flow shifting to a westward flow in the northern part. In Figure 2-l, the wind is moving toward the west, consistent with the observed northern part. However, the resolution of the model is too coarse to resolve the complex terrain and account for the wind direction.

With the estimation of the friction velocity, information on the flow regime can be evaluated, and the wavelength of dunes can be estimated (Courrech du Pont et al., 2024). The Reynolds number $R_r = r \cdot u_* / \nu$ with r the aerodynamic roughness height fixed to 1 cm and ν the viscosity of the atmosphere equal to $4 \cdot 10^{-7}$ m^2 s^{-1}, is superior to 100 on 98% of the domain. The flow is then in an aerodynamically rough regime, meaning that the viscous sublayer is perturbed by the turbulence mixing caused by the aerodynamic roughness height. In this regime, the minimum wavelength of the dunes is found to scale with the saturation length L_{sat}, equal to $4.4 \cdot d \cdot \rho_s / \rho_f$ (Claudin & Andreotti, 2006), with d the radius of the particle and ρ_p / ρ_f the ratio between the density of the particle and the density of the fluid. For the lowest saltation threshold, the particle radius is equal to 75μm with a ρ_p / ρ_f of 41 (Iversen & White, 1982), leading to a minimum wavelength of around 13 cm. The maximum wavelength of the dune would be of the order of the planetary boundary layer (PBL) height. No measurements exist of the turbulence at the surface of Venus. For the Venus PCM (Lebonnois et al., 2018) and Large Eddy Simulations (Lefèvre, 2022), on the Equatorial plains, the PBL height varies from a few hundred meters at night to around 1 km. On the high terrain, the PBL height can reach 7 km. At high latitudes, the PBL height would be below 1 km due to the weak solar flux.

6. Conclusion

In the next decade, there will be two radars (Ghail et al., 2018) on board Envision and VERITAS that will monitor the surface composition and geomorphological features. This study provides for the first time at a mesoscale level the near-surface dynamics of the Venusian atmosphere. It is shown that the main elevation features in the tropics control the dynamics in this region and that their vicinities are preferable locations for the sediment transport on Venus. The amplitude of 2 m-wind is 80% below 0.5 m s^{-1} and 95% below 1 m s^{-1}. This is consistent with the amplitude distribution deduced from measurements. The amplitude of the wind resolved by the model is in agreement with the VENERA measurements at the same local time. Due to the daytime solar heating and nighttime IR cooling, the wind amplitude and direction exhibit a clear diurnal cycle in the tropics, with the generation of slope winds. During the day, winds are going upslope, whereas at night they are going downslope. At the Poles, the solar flux at the surface is too small to induce anabatic winds during the day, resulting in constant katabatic winds on the largest slopes. These slope winds engendered by the thermal balance of the slope surface are thought to be ubiquitous in the tropics due to the absence of moist processes and seasonal effects and the stability of the cloud coverage.

The present modeling study reports the first estimate for Venus of the impact of slope winds on surface temperature. The slope winds impact the surface temperature diurnal amplitude, anabatic winds will cool down the environment, while katabatic winds will heat it up. On the low Equatorial plains, the surface temperature will vary by 4 K. However, on the slopes, the katabatic winds will heat the surface at a rate that the IR cooling cannot balance, resulting in a diurnal amplitude below 1 K. On Venus, the surface temperature in the tropics is therefore not only controlled by elevation but also by the slope.

The saltation of sediment by those winds was also estimated using the friction velocity formalism. The slope winds are dominating the near-surface dynamics, and a third of the domain in the tropics and almost half of the polar domain are above the lowest saltation threshold, that is for 75 μm particles, meaning that mesoscale winds are strong enough to lift dust of that size. These regions are close to mountain flanks, but flatter regions where you have wind convergence are also regions of saltation. However, the sediment reservoir is not known. One of the two regions where dune fields were observed is at the lowest saltation threshold level. Based on the value of the friction velocity, the flow is in a rough regime, leading to dune wavelengths between 13 cm and the PBL height, strongly varying with latitude, local time and height.

Several developments can improve the knowledge of the impact of slope winds in the Venusian environment. The heat capacity is set constant by design in the model. However, CO_2 heat capacity strongly varies with temperature (Lebonnois et al., 2010). Taking into account this peculiarity would provide a more realistic description of the stability of the atmosphere and the heating/cooling of slope winds.

The implementation of a thermal plume model to better represent subgrid turbulence, already in use for other planets, and tuned with future data, would be an additional refinement of the modeling.

This study considers surface properties such as emissivity, albedo, thermal inertia, and aerodynamic roughness height constant. Taking into account spatial variation of those characteristics depending on surface composition in future studies, like on Mars (Spiga & Forget, 2009), would provide a more realistic description of the Venusian near-surface dynamics.

Simulations at higher resolution and with a dust tracer should be performed to be able to assess the dust transport realistically.

Data Availability Statement

The Simulation outputs used to obtain the results in this paper are available in the open online repository (Lefèvre, 2025).

Acknowledgments
The authors would like to thank the two anonymous reviewers who helped to improve this study. This project has received funding from the European Union's Horizon Europe research and innovation program under the Marie Skłodowska-Curie Grant agreement 101110489/MuSICA-V. ML would like to acknowledge the use of the Sorbonne Université SACADO service unit.

References

Avduevskii, V. S., Vishnevetskii, S. L., Golov, I. A., Karpeiskii, I. I., Lavrov, A. D., Likhushin, V. I., et al. (1977). Measurement of wind velocity on the surface of Venus during the operation of stations Venera 9 and Venera 10. *Cosmic Research*, *14*(5), 710–713.

Blumberg, D. G., & Greeley, R. (1994). Venus: Influence of surface roughness on the threshold for windblown sand derived from Magellan data. In *Lunar and planetary science conference* (p. 129).

Bohachevsky, I. O. (1973). General atmospheric circulation driven by polar and diurnal surface temperature variations. *Icarus*, *19*(1), 118–125. https://doi.org/10.1016/0019-1035(73)90144-9

Bondarenko, N. V., Kreslavsky, M. A., & Head, J. W. (2006). North-south roughness anisotropy on Venus from the Magellan radar altimeter: Correlation with geology. *Journal of Geophysical Research (Planets)*, *111*(E6), E06S12. https://doi.org/10.1029/2005JE002599

Brossier, J. F., Gilmore, M. S., & Toner, K. (2020). Low radar emissivity signatures on Venus volcanoes and coronae: New insights on relative composition and age. *Icarus*, *343*, 113693. https://doi.org/10.1016/j.icarus.2020.113693

Claudin, P., & Andreotti, B. (2006). A scaling law for Aeolian dunes on Mars, Venus, Earth, and for subaqueous ripples. *Earth and Planetary Science Letters*, *252*(1–2), 30–44. https://doi.org/10.1016/j.epsl.2006.09.004

Courrech du Pont, S., Rubin, D. M., Narteau, C., Lapôtre, M. G. A., Day, M., Claudin, P., et al. (2024). Complementary classifications of Aeolian dunes based on morphology, dynamics, and fluid mechanics. *Earth-Science Reviews*, *255*, 104772. https://doi.org/10.1016/j.earscirev.2024.104772

Ford, P. G., & Pettengill, G. H. (1992). Venus topography and kilometer-scale slopes. *Journal of Geophysical Research*, *97*(E8), 13–13114. https://doi.org/10.1029/92JE01085

Forget, F., Hourdin, F., Fournier, R., Hourdin, C., Talagrand, O., Collins, M., et al. (1999). Improved general circulation models of the Martian atmosphere from the surface to above 80 km. *Journal of Geophysical Research*, *104*(E10), 24155–24176. https://doi.org/10.1029/1999JE001025

Garate-Lopez, I., & Lebonnois, S. (2018). Latitudinal variation of clouds' structure responsible for Venus' cold collar. *Icarus*, *314*, 1–11. https://doi.org/10.1016/j.icarus.2018.05.011

Garvin, J. B., Getty, S. A., Arney, G. N., Johnson, N. M., Kohler, E., Schwer, K. O., et al. (2022). Revealing the mysteries of Venus: The DAVINCI mission. *The Planetary Science Journal*, *3*(5), 117. https://doi.org/10.3847/PSJ/ac63c2

Ghail, R. C., Hall, D., Mason, P. J., Herrick, R. R., Carter, L. M., & Williams, E. (2018). VenSAR on EnVision: Taking Earth observation radar to Venus. *International Journal of Applied Earth Observation and Geoinformation*, *64*, 365–376. https://doi.org/10.1016/j.jag.2017.02.008

Gierasch, P. J., Goody, R. M., Young, R. E., Crisp, D., Edwards, C., Kahn, R., et al. (1997). The general circulation of the Venus atmosphere: An assessment. In *Venus II: Geology, geophysics, atmosphere, and solar wind environment* (p. 459).

Greeley, R., Arvidson, R. E., Elachi, C., Geringer, M. A., Plaut, J. J., Saunders, R. S., et al. (1992). Aeolian features on Venus - Preliminary Magellan results. *Journal of Geophysical Research*, *97*(E8), 13–13345. https://doi.org/10.1029/92JE00980

Gunn, A., & Jerolmack, D. J. (2022). Conditions for aeolian transport in the solar system. *Nature Astronomy*, *6*(8), 923–929. https://doi.org/10.1038/s41550-022-01669-0

Haus, R., Kappel, D., & Arnold, G. (2015). Radiative heating and cooling in the middle and lower atmosphere of Venus and responses to atmospheric and spectroscopic parameter variations. *Planetary and Space Science*, *117*, 262–294. https://doi.org/10.1016/j.pss.2015.06.024

Hernández-Bernal, J., Spiga, A., Sánchez-Lavega, A., del Río-Gaztelurrutia, T., Forget, F., & Millour, E. (2022). An extremely elongated cloud over arsia mons volcano on Mars: 2. Mesoscale modeling. *Journal of Geophysical Research: Planets*, *127*(10), e2022JE007352. https://doi.org/10.1029/2022JE007352

Hourdin, F., Couvreux, F., & Menut, L. (2002). Parameterization of the dry convective boundary layer based on a mass flux representation of thermals. *Journal of the Atmospheric Sciences*, *59*, 1105–1123. https://doi.org/10.1175/1520-0469(2002)059⟨1105:POTDCB⟩2.0.CO;2

Hourdin, F., Le van, P., Forget, F., & Talagrand, O. (1993). Meteorological variability and the annual surface pressure cycle on Mars. *Journal of the Atmospheric Sciences*, *50*, 3625–3640. https://doi.org/10.1175/1520-0469(1993)050⟨3625:MVATAS⟩2.0.CO;2

Iversen, J. D., Greeley, R., & Pollack, J. B. (1976). Windblown dust on Earth, Mars and Venus. *Journal of the Atmospheric Sciences*, *33*, 2425–2429. https://doi.org/10.1175/1520-0469(1976)033textless2425:WDOEMAtextgreater2.0.CO;2

Iversen, J. D., & White, B. R. (1982). Saltation threshold on Earth, Mars and Venus. *Sedimentology*, *29*(1), 111–119. https://doi.org/10.1111/j.1365-3091.1982.tb01713.x

Jakosky, B. M. (1984). Buffering of diurnal temperature variations on Venus. *Icarus*, *59*(3), 478–480. https://doi.org/10.1016/0019-1035(84)90115-5

Kerzhanovich, V. V., Mararov, Y. F., Marov, M. Y., Rozhdestvenskii, M. K., & Sorokin, V. P. (1980). Venera 11 and venera 12: Preliminary evaluations of wind velocity and turbulence in the atmosphere of Venus. *The Moon and the Planets*, *23*(3), 261–270. https://doi.org/10.1007/BF00902043

Kerzhanovich, V. V., & Marov, M. I. (1983). The atmospheric dynamics of Venus according to doppler measurements by the Venera entry probes. In *Venus* (pp. 766–778). The University of Arizona Press.

Knicely, J. J. C., Gilmore, M. S., Lynch, R. J., & Herrick, R. R. (2023). Strategies for safely landing on Venusian tesserae. *Planetary and Space Science*, *228*, 105652. https://doi.org/10.1016/j.pss.2023.105652

Kremic, T., Ghail, R., Gilmore, M., Hunter, G., Kiefer, W., Limaye, S., et al. (2020). Long-duration Venus lander for seismic and atmospheric science. *Planetary and Space Science*, *190*, 104961. https://doi.org/10.1016/j.pss.2020.104961

Ksanfomaliti, L. V., Goroshkova, N. V., & Khondyrev, V. K. (1983). Wind velocity on the Venus surface from acoustic measurements. *Kosmicheskie Issledovaniia*, *21*, 218–224.

Lange, L., Forget, F., Dupont, E., Vandemeulebrouck, R., Spiga, A., Millour, E., et al. (2023). Modeling slope microclimates in the Mars planetary climate model. *Journal of Geophysical Research: Planets*, *128*(10), e2023JE007915. https://doi.org/10.1029/2023JE007915

Lebonnois, S., Eymet, V., Lee, C., & Vatant d'Ollone, J. (2015). Analysis of the radiative budget of the Venusian atmosphere based on infrared net exchange rate formalism. *Journal of Geophysical Research: Planets*, *120*(6), 1186–1200. https://doi.org/10.1002/2015JE004794

Lebonnois, S., Hourdin, F., Eymet, V., Crespin, A., Fournier, R., & Forget, F. (2010). Superrotation of Venus' atmosphere analyzed with a full general circulation model. *Journal of Geophysical Research: Planets*, *115*(E6), E06006. https://doi.org/10.1029/2009JE003458

Lebonnois, S., Schubert, G., Forget, F., & Spiga, A. (2018). Planetary boundary layer and slope winds on Venus. *Icarus*, *314*, 149–158. https://doi.org/10.1016/j.icarus.2018.06.006

Lecacheux, J., Drossart, P., Laques, P., Deladerriére, F., & Colas, F. (1993). Detection of the surface of Venus at 1.0 *M* m from ground-based observations. *Planetary and Space Science*, *41*(7), 543–549. https://doi.org/10.1016/0032-0633(93)90035-Z

Lefèvre, M. (2022). Venus boundary layer dynamics: Eolian transport and convective vortex. *Icarus*, *387*, 115167. https://doi.org/10.1016/j.icarus.2022.115167

Lefèvre, M. (2025). The effect of near-surface winds on surface temperature and dust transport on Venus [Dataset]. *figshare*. https://doi.org/10.6084/m9.figshare.26063989

Lefèvre, M., Spiga, A., & Lebonnois, S. (2020). Mesoscale modeling of Venus' bow-shape waves. *Icarus*, *335*, 113376. https://doi.org/10.1016/j.icarus.2019.07.010

Lewis, J. S. (1971). Venus: Surface temperature variations. *Journal of the Atmospheric Sciences*, *28*(6), 1084–1085. https://doi.org/10.1175/1520-0469(1971)028⟨1084:VSTV⟩2.0.CO;2

Lorenz, R. D. (2016). Surface winds on Venus: Probability distribution from in-situ measurements. *Icarus*, *264*, 311–315. https://doi.org/10.1016/j.icarus.2015.09.036

Mahrt, L., & Larsen, S. (1990). Relation of slope winds to the ambient flow over gentle terrain. *Boundary-Layer Meteorology*, *53*(1–2), 93–102. https://doi.org/10.1007/BF00122465

McNider, R. T. (1982). A note on velocity fluctuations in drainage flows. *Journal of the Atmospheric Sciences*, *39*(7), 1658–1660. https://doi.org/10.1175/1520-0469(1982)039⟨1658:ANOVFI⟩2.0.CO;2

Mellor, G. L., & Yamada, T. (1982). Development of a turbulence closure model for geophysical fluid problems. *Reviews of Geophysics and Space Physics*, *20*(4), 851–875. https://doi.org/10.1029/RG020i004p00851

Mikkola, J., Sinclair, V. A., Bister, M., & Bianchi, F. (2023). Daytime along-valley winds in the Himalayas as simulated by the weather research and forecasting (WRF) model. *Atmospheric Chemistry and Physics*, *23*(2), 821–842. https://doi.org/10.5194/acp-23-821-2023

Montlaur, A., Arias, S., & Rojas, J. I. (2024). Thermally driven winds on Mars: A review and a slope effect numerical study. *Journal of Geophysical Research (Planets)*, *129*(4), e2023JE007987. https://doi.org/10.1029/2023JE007987

Moroz, V. I. (1983). Summary of preliminary results of the Venera 13 and Venera 14 missions. In *Venus* (pp. 45–68). The University of Arizona Press.

Mueller, N. T., Smrekar, S. E., & Tsang, C. C. C. (2020). Multispectral surface emissivity from VIRTIS on Venus express. *Icarus*, *335*, 113400. https://doi.org/10.1016/j.icarus.2019.113400

Nylen, T. H., Fountain, A. G., & Doran, P. T. (2004). Climatology of katabatic winds in the McMurdo dry valleys, southern Victoria Land, Antarctica. *Journal of Geophysical Research: Atmospheres*, *109*(D3), D03114. https://doi.org/10.1029/2003JD003937

Pettengill, G. H., Eliason, E., Ford, P. G., Loriot, G. B., Masursky, H., & McGill, G. E. (1980). Pioneer Venus radar results - Altimetry and surface properties. *Journal of Geophysical Research*, *85*(A13), 8261–8270. https://doi.org/10.1029/JA085iA13p08261

Rafkin, S. C. R., Pla-Garcia, J., Kahre, M., Gomez-Elvira, J., Hamilton, V. E., Marín, M., et al. (2016). The meteorology of Gale Crater as determined from rover environmental monitoring station observations and numerical modeling. Part II: Interpretation. *Icarus*, *280*, 114–138. https://doi.org/10.1016/j.icarus.2016.01.031

Richardson, M. I., & Newman, C. E. (2018). On the relationship between surface pressure, terrain elevation, and air temperature. Part I: The large diurnal surface pressure range at Gale Crater, Mars and its origin due to lateral hydrostatic adjustment. *Planetary and Space Science*, *164*, 132–157. https://doi.org/10.1016/j.pss.2018.07.003

Richardson, M. I., Toigo, A. D., & Newman, C. E. (2007). PlanetWRF: A general purpose, local to global numerical model for planetary atmospheric and climate dynamics. *Journal of Geophysical Research: Planets*, *112*(E9), E09001. https://doi.org/10.1029/2006JE002825

Schmidli, J., Böing, S., & Fuhrer, O. (2018). Accuracy of simulated diurnal valley winds in the Swiss alps: Influence of grid resolution, topography filtering, and land surface datasets. *Atmosphere*, *9*(5), 196. https://doi.org/10.3390/atmos9050196

Skamarock, W. C., & Klemp, J. B. (2008). A time-split nonhydrostatic atmospheric model for weather research and forecasting applications. *Journal of Computational Physics*, *227*(7), 3465–3485. https://doi.org/10.1016/j.jcp.2007.01.037

Spiga, A. (2011). Elements of comparison between Martian and terrestrial mesoscale meteorological phenomena: Katabatic winds and boundary layer convection. *Planetary and Space Science*, *59*(10), 915–922. https://doi.org/10.1016/j.pss.2010.04.025

Spiga, A., & Forget, F. (2009). A new model to simulate the Martian mesoscale and microscale atmospheric circulation: Validation and first results. *Journal of Geophysical Research: Planets*, *114*(E2), E02009. https://doi.org/10.1029/2008JE003242

Spiga, A., Forget, F., Madeleine, J.-B., Montabone, L., Lewis, S. R., & Millour, E. (2011). The impact of Martian mesoscale winds on surface temperature and on the determination of thermal inertia. *Icarus*, *212*(2), 504–519. https://doi.org/10.1016/j.icarus.2011.02.001

Spiga, A., & Smith, I. (2018). Katabatic jumps in the Martian northern polar regions. *Icarus*, *308*, 197–208. https://doi.org/10.1016/j.icarus.2017.10.021

Stone, P. H. (1975). The dynamics of the atmosphere of Venus. *Journal of the Atmospheric Sciences*, *32*(6), 1005–1016. https://doi.org/10.1175/1520-0469(1975)032⟨1005:TDOTAO⟩2.0.CO;2

Strezoski, A., & Treiman, A. H. (2022). The "Snow Line" on Venus's Maxwell montes: Varying elevation implies a dynamic atmosphere. *The Planetary Science Journal*, *3*(12), 264. https://doi.org/10.3847/PSJ/ac9f3a

Treiman, A., Harrington, E., & Sharpton, V. (2016). Venus' radar-bright highlands: Different signatures and materials on Ovda Regio and on Maxwell Montes. *Icarus*, *280*, 172–182. https://doi.org/10.1016/j.icarus.2016.07.001

Weitz, C. M., Plaut, J. J., Greeley, R., & Saunders, R. S. (1994). Dunes and microdunes on Venus: Why were so few found in the Magellan data? *Icarus*, *112*(1), 282–295. https://doi.org/10.1006/icar.1994.1181